Inorganic Chemistry
Cite This: Inorg. Chem. XXXX, XXX, XXX−XXX
Article
pubs.acs.org/IC

Affinity-Enhanced Luminescent Re(I)- and Ru(II)-Based Inhibitors of the Cysteine Protease Cathepsin L

Matthew Huisman,[†] Jacob P. Kodanko,[†] Karan Arora,[†] Mackenzie Herroon,[‡] Marim Alnaed,[†] John Endicott,[†] Izabela Podgorski,[‡,§] and Jeremy J. Kodanko*[,†,§]

[†]Department of Chemistry, Wayne State University, 5101 Cass Avenue, Detroit, Michigan 48202, United States
[‡]Department of Pharmacology, School of Medicine, Wayne State University, Detroit, Michigan 48201, United States
[§]Barbara Ann Karmanos Cancer Institute, Detroit, Michigan 48201, United States

Supporting Information

ABSTRACT: Two new Re(I)- and Ru(II)-based inhibitors were synthesized with the formulas [Re(phen)(CO)$_3$(**1**)](OTf) (**7**; phen = 1,10-phenanthroline, OTf = trifluoromethanesulfonate) and [Ru(bpy)$_2$(**2**)](Cl)$_2$ (**8**; bpy = 2,2′-bipyridine), where **1** and **2** are the analogues of CLIK-148, an epoxysuccinyl-based cysteine cathepsin L inhibitor (CTSL). Compounds **7** and **8** were characterized using various spectroscopic techniques and elemental analysis; **7** and **8** both show exceptionally long excited state lifetimes. Re(I)-based complex **7** inhibits CTSL in the low nanomolar range, affording a greater than 16-fold enhancement of potency relative to the free inhibitor **1** with a second-order rate constant of 211000 ± 42000 M^{-1} s^{-1}. Irreversible ligation of **7** to papain, a model of CTSL, was analyzed with mass spectroscopy, and the major peak shown at 24283 au corresponds to that of papain-**1**-Re(CO)$_3$(phen). Compound **7** was well tolerated by DU-145 prostate cancer cells, with toxicity evident only at high concentrations. Treatment of DU-145 cells with **7** followed by imaging via confocal microscopy showed substantial intracellular fluorescence that can be blocked by the known CTSL inhibitor CLIK-148, consistent with the ability of **7** to label CTSL in living cells. Overall this study reveals that a Re(I) complex can be attached to an enzyme inhibitor and enhance potency and selectivity for a medicinally important target, while at the same time allowing new avenues for tracking and quantification due to long excited state lifetimes and non-native element composition.

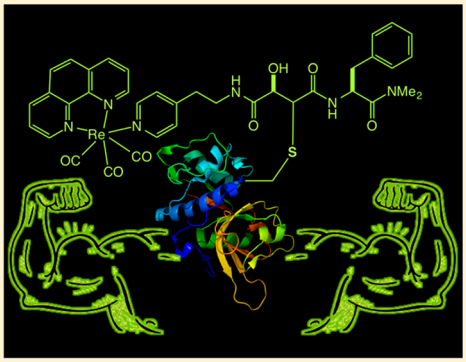

INTRODUCTION

Cysteine cathepsins are proteases that play a major role in normal cellular physiology and also in pathogenesis. A total of 11 family members of cysteine cathepsins have been characterized to date.[1] Aberrant activity and overexpression of cysteine cathepsins are associated with many human disease states.[2,3] Because of the crucial role of these proteases in biology, their inhibitors have been pursued aggressively by academic laboratories and also by pharmaceutical companies, as chemical tools to understand the role of cysteine proteases in biology and also as pharmaceuticals.[4−6]

Cathepsin L (CTSL) is a lysosomal cysteine protease that is upregulated in some cancers,[7] neurodegenerative disorders, atherosclerosis,[8,9] and inflammation.[10,11] Because of its higher expression levels in diseased tissues, CTSL can be used for diagnostic purposes. For instance, cysteine proteases are significantly more abundant in malignant vs benign glioma tumors where, in contrast to cathepsin B (CTSB) found in the tumor and tumor-associated endothelial cells, immunohistochemical staining reveals selective localization of CTSL to tumor cells only.[12] Overall, CTSL inhibitors have significant potential therapeutic value, especially as adjuvants to current therapies.[7,13,14] In addition, small molecules that carry reporters such as fluorophores for detecting active cysteine cathepsins, including CTSL, have applications in in vivo and ex vivo detection and diagnosis of human diseases.[15−17]

Research in the area of cysteine protease inhibition has been dominated by purely organic compounds.[4,5,14,18,19] Most inhibitors were designed to carry a reactive functional group or "warhead" that creates a covalent bond with the enzyme upon attack by the active site cysteine thiolate. This includes epoxysuccinyl-based inhibitors of CTSL, such as CLIK-148 (Figure 1), which block the action of this protease in vitro and in vivo through selective binding and covalent modification by epoxide-opening reactions.[4,20] Metal-based protease inhibitors are much more rare,[21] although good progress has been made identifying Pd(II),[22,23] Au(III),[22,24] and Re(V)[25,26] complexes with low micromolar to nanomolar potentcies against cysteine proteases such as CTSB. In particular, Au(III)-based compounds that interact directly with the active site thiolate of cysteine proteases have shown activity in preclinical cancer models.[27,28] For all of these compounds, the metal is

Received: April 12, 2018

DOI: 10.1021/acs.inorgchem.8b00978
Inorg. Chem. XXXX, XXX, XXX−XXX

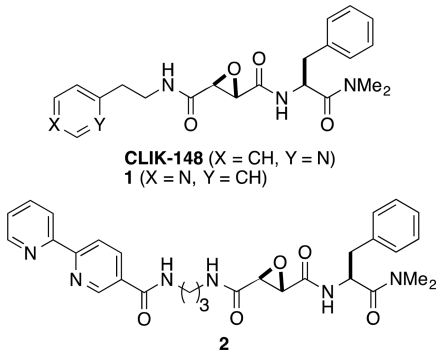

Figure 1. Structures of epoxysuccinyl-based cysteine cathepsin inhibitors.

considered to be the warhead that binds directly to the active site thiolate.

Re(I) and Ru(II) fluorogenic metal fragments have many applications in the labeling and detection of biomolecules.[29,30] These fluorophores are attractive because they show several advantages over more traditional organic emitters, including long-lived excited states that can be used in time-gated imaging experiments, enhanced resistance to photobleaching, and compositions containing non-native elements, making detection and quantification by ICP-MS straightforward.[29,31,32] In addition, Re(I) tricarbonyl compounds can be tracked by IR-based spectromicroscopy, a new type of cell imaging.[33] While tagging biologically active molecules with fluorophores allows for visualization and tracking targets of interest, the fluorophore has traditionally provided no real advantage toward gaining higher potency or selectivity between related targets.

In this paper, we report CTSL inhibitors bearing Re(I) and Ru(II) metal centers that not only luminesce but also show enhanced affinity and selectivity for inhibition of CTSL over other enzymes in this family. Importantly, this study reveals a new strategy for using coordinatively saturated metal complexes to enhance potency through favorable noncovalent interactions with protein targets. Both compounds show significantly longer lived excited states in comparison to more traditional organic fluorophores, which makes them appropriate for time-gated imaging experiments. Furthermore, we report a Re(I)-based inhibitor that is cell permeable and nontoxic at nanomolar and low micromolar concentrations. Our data are consistent with this Re(I) inhibitor labeling CTSL in living prostate cancer cells.

EXPERIMENTAL SECTION

General Considerations. NMR spectra were recorded on a Varian FT-NMR Mercury 400 MHz spectrometer. Mass spectra were recorded on a time-of-flight Micromass LCT Premier XE spectrometer. IR spectra were recorded on a Nicolet FT-IR spectrophotometer (thin film). UV−vis spectra were recorded on a Varian Cary 50 spectrophotometer. All reactions were performed an under ambient atmosphere unless otherwise noted. Anaerobic reactions were performed by purging the reaction solutions with Ar or N_2.

Synthesis. *(2S,3S)-N²-(3-([2,2′-Bipyridine]-5-carboxamido)-propyl)-N³-(1-(dimethylamino)-1-oxo-3-phenylpropan-2-yl)-oxirane-2,3-dicarboxamide (**2**).* A solution of (2*S*,3*S*)-3-(((*S*)-1-(dimethylamino)-1-oxo-3-phenylpropan-2-yl)carbamoyl)oxirane-2-carboxylic acid (**6**;[34] 477 mg, 1.56 mmol) and *p*-nitrophenol (217 mg, 1.56 mmol) in EtOAc (4.5 mL) was maintained at 0 °C for 5 min under a nitrogen atmosphere. A solution of DCC (331 mg, 1.60 mmol) in EtOAc (4.5 mL) was added dropwise over a period of 30 min. The reaction mixture was warmed to room temperature and stirred overnight for 18 h. After consumption of the starting material, as judged by TLC analysis, the reaction mixture was filtered through Celite. The solvent was evaporated in vacuo to obtain the *p*-nitrophenol ester as a crude yellow solid (675 mg). The *p*-nitrophenol ester was analyzed by ^{1}H NMR and TLC, showing only *p*-nitrophenol as a minor impurity, and was used without further purification. Data for the ester are as follows: R_f = 0.4, silica, 1/1 hexane/EtOAc; ^{1}H NMR (400 MHz, $CDCl_3$) δ 8.32 (d, J = 8.9 Hz, 2H), 7.35−7.29 (m, 5H), 7.17 (d, J = 8.1 Hz, 2H), 6.99 (d, J = 8.1 Hz, 1H), 6.92 (d, J = 8.9 Hz, 2H), 5.16 (dd, J = 14.6, 8.1 Hz, 1H), 3.78 (d, J = 2.0 Hz, 1H), 3.50 (d, J = 2.0 Hz, 1H), 3.08−3.02 (m, 1H), 2.99−2.96 (m, 1H), 2.93 (s, 3H), 2.76 (s, 3H).

The crude *p*-nitrophenol ester (358 mg, 0.837 mmol) in dry CH_2Cl_2 (6 mL) was maintained at room temperature for 5 min under a nitrogen atmosphere. *N*-(3-Aminopropyl)-[2,2′-bipyridine]-5-carboxamide (**5**; 195 mg, 0.761 mmol) in CH_2Cl_2 (6 mL) was added dropwise over a period of 20 min. The reaction mixture was maintained under a nitrogen atmosphere for 16 h at room temperature. After consumption of the starting material, as judged by TLC analysis, the organic layer was evaporated in vacuo to give a crude mixture which was purified by silica gel chromatography (0−20% MeOH/EtOAc) to afford the product **2** as a white solid (244 mg, 59% over two steps). Data for **2** are as follows: ^{1}H NMR (400 MHz, CD_3OD) δ 9.08 (d, J = 1.5 Hz, 1H), 8.68 (d, J = 4.4 Hz, 1H), 8.41 (m, 2H), 8.32 (dd, J = 8.3, 2.5 Hz, 1H), 7.96 (dt, J = 7.8, 1.5 Hz, 1H), 7.47 (dd, J = 4.9, 2.5 Hz, 1H), 7.31−7.28 (m, 2H), 7.25−7.21 (m, 3H), 5.08 (t, J = 7.3 Hz, 1H), 3.61 (d, J = 2.0 Hz, 1H), 3.47−3.43 (m, 3H), 3.35−3.32 (m, 2H), 3.06−3.01 (m, 1H), 2.98−2.92 (m, 1H), 2.84 (s, 3H), 2.82 (s, 3H), 1.82 (p, J = 6.9 Hz, 2H); $[\alpha]_{D25}$ +51 (c = 1.0, MeOH); ^{13}C NMR (100 MHz, CD_3OD) δ 171.2, 167.4, 166.6, 166.5, 158.0, 154.9, 149.1, 148.0, 137.3, 136.2, 135.9, 129.9, 129.0, 128.1, 126.7, 124.4, 121.6, 120.4, 53.4, 53.1, 50.6, 37.7, 36.9, 36.1, 34.7, 28.6; IR (thin film) 3278, 3063, 2934, 1629, 1589, 1538, 1456, 1435, 1297, 1249, 1145, 1091, 1023, 992, 893, 807, 759, 700, 639, 618, 523, 496 cm^{-1}; HRMS (ESMS) calculated for $C_{29}H_{32}N_6O_5$ $[M + H]^+$ 545.2434, found 545.2512.

*Methyl [2,2′-Bipyridine]-5-carboxylate (**4**).* A solution of methyl 6-chloronicotinate (1.00 g, 5.83 mmol) and pyridin-2-ylzinc(II) bromide (17.48 mL, 8.74 mmol, 0.5 M in THF) was maintained at room temperature, and argon was bubbled through the solution for 20 min. Tetrakis(triphenylphosphine)palladium(0) (337 mg, 0.291 mmol) was added to the mixture, and the vessel with this mixture was sealed under an inert atmosphere, wrapped in aluminum foil, and heated to 65 °C for 16 h. The reaction mixture was a tan-yellow suspension which was poured into aqueous 10% EDTA solution (50 mL) and stirred for 15 min, and then saturated Na_2CO_3 was added to achieve pH ∼8. The product was extracted with CH_2Cl_2 (3 × 28 mL) and dried over Na_2SO_4, and solvent was evaporated in vacuo to obtain the crude product. The crude mixture was purified by silica gel chromatography (0−10% EtOAc/hexanes) to afford **4** as a white solid (1.01 g, 81%). ^{1}H NMR and ESMS spectral data for **4** were in good agreement with data from the literature.[35]

*N-(3-Aminopropyl)-[2,2′-bipyridine]-5-carboxamide (**5**).* A solution of **4** (1.01 g, 4.71 mmol) and propane-1,3-diamine (4.79 mL, 4.25 g 55.2 mmol) in MeOH (80 mL) was refluxed for 18 h under a nitrogen atmosphere. After consumption of the starting material, as judged by TLC analysis, the reaction mixture was concentrated under reduced pressure and excess 1,3-propanediamine was removed by azeotropic distillation from toluene (3 × 60 mL) to give compound **5** as a white solid (1.01 g 83%). Data for **5** are as follows: ^{1}H NMR (400 MHz, CD_3OD) δ 9.07 (d, J = 1.5 Hz, 1H), 8.68 (d, J = 4.4 Hz, 1H), 8.43−8.40 (m, 2H), 8.31 (dd, J = 8.3, 2.5 Hz, 1H), 7.96 (dt, J = 7.8, 1.5 Hz, 1H), 7.47 (dd, J = 4.9, 2.5 Hz, 1H), 3.50 (t, J = 6.9 Hz, 2H), 2.77 (t, J = 6.9 Hz, 2H), 1.82 (p, J = 6.9 Hz, 2H); ^{13}C NMR (100 MHz, CD_3OD) δ 166.6, 158.0, 154.9, 149.1, 148.0, 137.3, 135.9, 129.9, 124.4, 121.6, 120.4, 38.2, 36.9, 31.4; IR (thin film): 3294, 3060, 3003, 2952, 2919, 2872, 1629, 1589, 1536, 1479, 1456, 1434, 1422, 1367, 1331, 1287, 1249, 1151, 1121, 1089, 1015, 995, 860, 849, 756, 664, 637, 617, 592, 510, 492 cm^{-1}; HRMS (ESMS) calculated for $C_{14}H_{16}N_4O$ $[M + H]^+$ 257.1324, found 257.1400.

DOI: 10.1021/acs.inorgchem.8b00978
Inorg. Chem. XXXX, XXX, XXX−XXX

*[Re(Phen)(CO)$_3$(**1**)](OTf) (**7**).* In a sealable tube, a solution of **1**[34] (191 mg, 0.470 mmol) and $CHCl_3$/MeOH (4.5/18 mL) was maintained at room temperature and argon was bubbled through the solution for 20 min. Re(1,10-phenanthroline)(CO)$_3$(OTf)[36] (210 mg, 0.350 mmol) was added to the mixture, and the tube containing the mixture was sealed under an inert atmosphere, wrapped in aluminum foil, and heated to 60 °C for 16 h. The solvent was removed in vacuo without external heating, resulting in a yellow solid. The resulting 419 mg of solid was purified using silica gel chromatography (0−10% MeOH/CH_2Cl_2) to give a yellow solid after solvent removal: 178 mg; R_f = 0.4, silica gel, 9/1 CH_2Cl_2/MeOH. The precipitate was dissolved in a small amount of MeOH (0.5 mL) and layered with Et_2O (10 mL). After this solution was stored at −20 °C for 16 h, the complex precipitated as a yellow solid. The solution was decanted, and layering was repeated two more times. The solid was isolated by scraping and dried in vacuo to provide Re(Phen)(CO)$_3$(1)(OTf) (**7**) as a microcrystalline yellow solid (162 mg, 50%). Data for **7** are as follows: mp 137 °C; ^{1}H NMR (400 MHz, CD_3OD) δ 9.73 (d, J = 5.4 Hz, 2H), 8.93−8.90 (m, 2H), 8.29 (d, J = 6.4 Hz, 2H), 8.20−8.16 (m, 4H), 7.32−7.21 (m, 5H), 7.11 (d, J = 6.4 Hz, 2H), 5.06 (t, J = 7.3 Hz, 1H), 3.28−3.26 (m, 2H), 3.25 (d, J = 1.5 Hz, 1H), 3.14 (d, J = 1.5 Hz, 1H), 3.04 (dd, J_1 = 13.4 Hz, J_2 = 7.2 Hz, 1H), 2.94 (dd, J_1 = 13.4 Hz, J_2 = 7.7 Hz, 1H), 2.88 (s, 3H), 2.85 (s, 3H), 2.68 (t, J = 6.6 Hz, 2H); IR (thin film) 3547, 3296, 3065, 2934, 2029, 1906, 1678, 1639, 1520, 1429, 1281, 1223, 1152, 1028, 897, 849, 723, 702, 637, 573, 540, 517, 484, 420 cm^{-1}; HRMS (ESMS) calcd for $C_{38}H_{34}N_6O_7Re$ $[M]^+$ 861.2046, found 861.1794; UV−vis λ_{max} 275 nm (ε = 33300 M^{-1} cm^{-1}), λ_{em} 543 nm. Anal. Calcd for $C_{38}H_{34}F_3N_6O_{10}ReS$ (7·2H_2O): C, 43.63; H, 3.66; N, 8.03. Found: C, 43.89; H, 3.62; N, 7.92.

*[Ru(bpy)$_2$(**2**)](Cl)$_2$ (**8**).* In a sealable tube, a solution of **2** (40 mg, 0.074 mmol) and EtOH (15 mL) was maintained at room temperature and argon was bubbled through the solution for 20 min. The compound *cis*-[Ru(bpy)$_2$Cl$_2$][37] (30 mg, 0.062 mmol) was added, and the tube containing the mixture was sealed under an inert atmosphere, wrapped in aluminum foil, and heated to 80 °C for 16 h, during which time the mixture turned from dark violet to bright orange. After the mixture was cooled to room temperature, the solvent was removed in vacuo without external heating, resulting in an orange solid. The solid was dissolved in a small amount of MeOH (0.5 mL) and layered with Et_2O (10 mL). After this solution was stored at −20 °C for 16 h, the complex precipitated as an orange solid. The solution was decanted, and layering was repeated two more times. The solid was isolated by scraping and dried in vacuo to provide compound **8** as a microcrystalline orange solid (29 mg, 38%). Data for **8** are as follows: mp 154 °C; ^{1}H NMR (400 MHz, CD_3OD) δ 8.78 (t, J = 8.8 Hz, 2H), 8.72−8.68 (m, 4H), 8.46−8.43 (m, 1H), 8.18−8.09 (m, 6H), 7.88−7.83 (m, 3H), 7.80 (t, J = 5.4 Hz, 2H), 7.54−7.45 (m, 5H), 7.32−7.28 (m, 2H), 7.26−7.22 (m, 3H), 5.08 (td, J = 7.4, 2.0 Hz, 1H), 3.51 (t, J = 2.0 Hz, 1H), 3.38 (d, J = 2.0 Hz, 1H), 3.20−3.12 (m, 2H), 3.07−3.02 (m, 1H), 2.98−2.93 (m, 1H), 2.85 (s, 3H), 2.83 (s, 3H), 1.75−1.68 (m, 2H); IR (thin film) 3379, 3229, 3063, 2934, 1638, 1601, 1535, 1462, 1443, 1304, 1271, 1242, 1159, 893, 764, 729 cm^{-1}; HRMS (ESMS) calcd for $C_{49}H_{46}N_{10}O_5Ru$ $[M]^{2+}$ 479.1433, found 479.1399; UV−vis λ_{max} 449 nm (ε = 8200 M^{-1} cm^{-1}), λ_{em} 631 nm. Anal. Calcd for $C_{49}H_{48}Cl_2N_{10}O_5Ru$ (**8**·7H_2O): C, 50.95; H, 5.41; N, 12.13. Found: C, 50.66; H, 5.31; N, 11.84.

Lifetime Measurements. The 77 K emission lifetimes were determined using a Spectra Physics VSL-337ND-S nitrogen laser-pumped DUO-210 Dye laser system, Hamamatsu P9220 PMT/E717-63 mounted on a Jobin-Yvon H-100 spectrometer with a National Instruments NI PCI-5154, 2 GS/s, 1 GHz Digitizer w/8 MB/ch onboard memory PC card as described previously.[38] The laser had about a 5 ns pulse width, and the instrument response to scattered excitation light was experimentally determined to have a 1/e decay time of 9 ± 2 ns. Aqueous sample solutions contained 50 mM potassium phosphate buffer (pH 7.4) and 10% DMSO.

Enzyme Inhibition. Progress curves for release of free 7-amino-4-methylcoumarin (AMC) by CTSL were collected using CTSL (4 nM), *Z*-Phe-Arg-AMC (10 μM), **1**, **2**, **7**, and **8** (0.05−2.5 μM) in 0.4 M acetate buffer, pH 5.5, <1% DMSO, 4 mM EDTA, 0.01% Triton X-100, and DTT 8 mM at 25 °C as described previously.[34] Cathepsin S inhibition data were collected using CTSS (4 nM), *Z*-Val-Val-Arg-AMC (10 μM), **1**, **2**, **7**, and **8** (1−20 μM) in 50 mM phosphate buffer, pH 6.5, <1% DMSO, 2.5 mM EDTA, and DTT 8 mM at 25 °C. Cathepsin B inhibition data were collected using CTSB (4 nM), *Z*-Arg-Arg-AMC (10 μM), **1**, **2**, **7**, and **8** (1 nM to 100 μM) in 0.4 M acetate buffer, pH 5.5, <1% DMSO, 5 mM EDTA, 0.01% Triton X-100, and DTT 10 mM at 25 °C. CA-074 was used as a positive control for CTSB inhibition. Data are averages of three independent experiments with errors equal to standard deviations. Progress curve data were analyzed using the program Dynafit[39] to obtain k_{inact} and K_i values using a literature method.[34]

Papain Rhenium Complex MS Analysis. A concentrated solution of papain (from papaya latex, Sigma-Aldrich, P4762) was prepared in 20% DMSO/H_2O (20 mg/mL), resulting in a suspension that was filtered through a 0.2 μM membrane. The filtrate (50 μL) was added to a solution of L-cysteine hydrochloride (2 mg/mL, 200 μL) and inhibitor **7** (2 mg/mL, 200 μL) in the dark. The solution was incubated at room temperature for 18 h in the dark and was concentrated to a volume of ∼50 μL using a 10 kDa centrifugal filter (Amicon Ultra Ultracel 10K membrane) at 4 °C and 14000*g* for 30 min. The sample was diluted in 0.2% AcOH/H_2O (400 μL) and concentrated to ∼50 μL. This cycle was repeated four times to remove excess **7** and L-cysteine. The sample was diluted to a final volume of 450 μL in 0.2% AcOH/H_2O and injected (10 μL) into a Waters LCT Premier XE Micromass KD128 time-of-flight mass spectrometer with an electrospray source. Spectra were collected from m/z 1000 to 2000, and the signal was deconvoluted using Masslynx.

Lysate Studies. Lysates obtained from DU-145 and ARCaP(M) prostate cancer cells were diluted 4× with activating buffer (0.4 M acetate buffer, 4 mM EDTA, pH 5.5, DTT 8 mM) and incubated for 20 min at room temperature. The substrate *Z*-Phe-Arg-AMC (100 μM) in assay buffer was added, and the fluorescence of hydrolyzed AMC was recorded as a function of time. Lysates were incubated with 5−30 μM [Re(phen)(CO)$_3$(**1**)](OTf) (**7**) for 15 min and then loaded directly onto the gel or heated for 5 min at 100 °C and analyzed by SDS PAGE gel analysis using a Criterion TGX instrument with 4−20% SDS gradient gel with and 302 nm excitation on a UV transilluminator.

Cell Studies. The viability effects of **7** on DU-145 cells were tested via the MTT assay according to the manufacturer's instructions (Invitrogen, Waltham, MA). Briefly, DU-145 cells were plated in 96-well plates (Invitrogen/Thermo Fisher Scientific, Waltham, MA) at 5 × 10^3 cells per well in 100 μL of DMEM containing 10% FBS. One plate was seeded for "UV" conditions and one plate for "dark" conditions. After 24 h of growth, cells were treated in the dark with an increasing concentration of **7** (supplied in 100 μL of media with the final DMSO concentration kept at 0.5%), and eight biological replicates for each concentration were tested per plate. The plates were loosely wrapped with aluminum foil and placed back in the incubator for a 2 h incubation at 37 °C, after which both plates were removed and set at room temperature for 40 min while the "light" plate was unwrapped and exposed to UV light. The lamp used was a 4 W long-wave UV (365 nm) light, powered at 115 V (UVP, Upland, CA). Following irradiation, the cells were placed back in the incubator and kept in the dark under a 5% CO_2 atmosphere at 37 °C for another 48 h. Following the required incubation, the medium was removed and 100 μL of fresh medium per well was added followed by the addition of 10 μL of a 12 mM MTT stock solution (5 mg of MTT dissolved in 1 mL of sterile PBS). A negative control consisting of 100 μL of medium plus 10 μL of MTT solution was added to empty wells. The dishes were rewrapped and placed back into the incubator for 4 h. Medium solution (85 μL) was then removed from each well, and 50 μL of DMSO was added, followed by rocking the plate to ensure thorough mixing. Cells were incubated at 37 °C for another 10 min before reading the absorbance at 540 nm on a plate reader.

Confocal Analysis of Rhenium Compounds in Cells. To measure the uptake of the rhenium compound by DU-145 cells, we applied live imaging techniques. Cells were plated in 35 mm dishes (200000/dish) in DMEM containing 10% FBS and kept in a 37 °C

DOI: 10.1021/acs.inorgchem.8b00978
Inorg. Chem. XXXX, XXX, XXX−XXX

humidified incubator ventilated with 5% CO_2, in line with recommended growth conditions for these cells. After 48 h of growth, cells were treated with 30 μM of the Re(I) compound 7 or with vehicle (DMSO, blank). The DMSO concentration was kept at 0.1% of the total volume. Cells were incubated for 2 h and then removed and gently washed three times with PBS. Cells were kept in PBS for the duration of confocal imaging. Briefly, images of cells were captured using a Zeiss LSM 780 confocal microscope (Carl Zeiss AG, Göttingen, Germany) using both 20× and 40× water immersion lenses. Excitation was set at 405 nm using a diode laser, with the dichroic filter set at 405/505 nm. All emission from 501 to 740 nm was collected. Z-stack images (1.5 μm optical slices) of the cells were taken to capture the complete fluorescence available as opposed to being limited to a single plane. Four biological replicates per condition were imaged at 20× to measure the integrated intensity. Intensities of the images were measured via Volocity software (PerkinElmer, Waltham, MA), and the integrated intensity per image was quantified by dividing the total sum of the fluorescence signal (thresholded using intensity) by the number of cells per image (counted manually). 3D reconstructed images showing the fluorescence were constructed using Volocity software.

Assessment of the Effect of Cathepsin L Inhibition on Rhenium Compound Uptake. We followed a similar procedure to measure the inhibitory effect of CTSL inhibitor CLIK-148 on the uptake of the rhenium compound by DU-145 cells. Cells were plated in 35 mm dishes (150000/dish) under normal growth conditions. After 48 h of culture, cells were treated with 50 μM of CLIK-148 or with vehicle (0.5%, DMSO, blank). Cells were incubated with the inhibitor for 24 h, and then the medium was removed and cells were gently washed three times with PBS. Cells were then treated with 30 μM of the rhenium compound or vehicle (0.3%, DMSO) and incubated with the compound for 2 h. Before confocal analysis, the medium was removed and cells were gently washed three times with PBS and maintained in PBS for the duration of the imaging protocol. Confocal analysis was performed as described above for uptake studies.

RESULTS AND DISCUSSION

Epoxysuccinyl-based inhibitors **1** and **2** were synthesized to create Re(I) and Ru(II) conjugates. Compound **1** was obtained following a literature protocol in 10 steps total from D-tartaric acid.[34,40,41] Inhibitor **2** was prepared by starting from methyl 6-chloronicotinate (**3**; Scheme 1A). 2-Pyridylzinc bromide and methyl 6-chloronicotinate were coupled using a modified Negishi cross-coupling protocol to obtain the desired intermediate methyl [2,2′-bipyridine]-4-carboxylate (**4**).[35] Compound **4** was converted to an amide upon treatment with excess propane-1,3-diamine in refluxing methanol to form **5** in good yield (83%). To complete the synthesis of **2**, the advanced intermediate **6**,[34] available in 8 steps from D-tartaric acid (Scheme 1B), was treated with *p*-nitrophenol and dicyclohexylcarbodimide (DCC), resulting in the formation of an activated *p*-nitrophenyl ester that was combined with **5** to give **2** in 59% yield over the two steps.

Scheme 1. Synthesis of Epoxysuccinyl Inhibitor 2

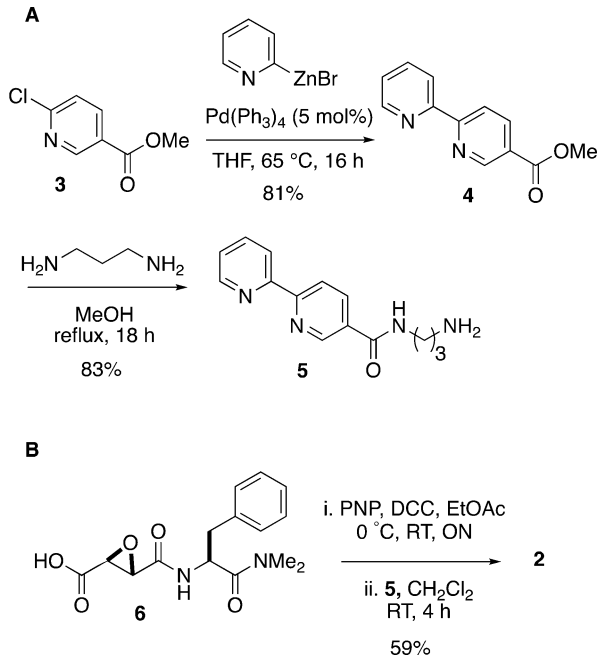

Scheme 2. Synthesis of Luminescent Re(I)-Based (A) and Ru(II)-Based (B) Epoxysuccinyl Inhibitors

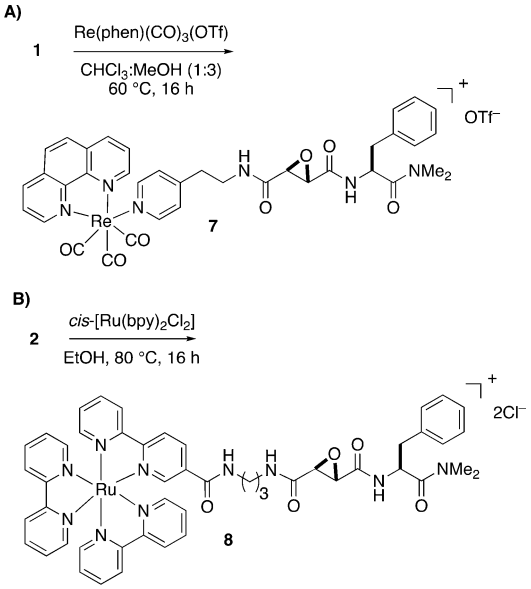

Syntheses of the Re(I)- and Ru(II)-based inhibitors are shown in parts A and B, respectively, of Scheme 2. The CLIK analogue **1** was treated with $Re(phen)(CO)_3OTf$[36] in $CHCl_3$/MeOH, giving the Re(I) conjugate **7** in 50% yield after precipitation from MeOH/Et_2O. Heating inhibitor **2** in the presence of *cis*-$[Ru(bpy)_2Cl_2]$[37] in EtOH for 16 h, followed by layering in MeOH/Et_2O, gave Ru(II) conjugate **8** in 38% yield.

Spectroscopic Characterization. Metal complexes **7** and **8** were characterized by ^{1}H NMR, IR, electronic absorbance, and fluorescence emission spectroscopy, electrospray mass spectrometry, and elemental analysis. Mass spectra for **7** and **8** show ion clusters with prominent peaks at m/z 861.2 and 479.1, respectively, along with suitable isotopic patterns consistent with those expected for the monocation $[Re(phen)(CO)_3(\mathbf{1})]^+$ and dication $[Ru(bpy)_2(\mathbf{2})]^{2+}$ (Figures S6 and S9). The Re(I) conjugate **7** shows electronic absorption (λ_{max} 275 nm, ε = 33300 M^{-1} cm^{-1}) and emission (λ_{em} 543 nm) spectra consistent with other compounds containing the $Re(phen)(CO)_3$ fragment with bound monodentate pyridines (Figure 2).[42] Ru(II) conjugate **8** shows absorption (λ_{max} 449 nm, ε = 8200 M^{-1} cm^{-1}) and emission (λ_{em} 631 nm) bands consistent with the $Ru(bpy)_3^{2+}$ fragment.[43]

^{1}H NMR and IR spectroscopic analyses were used to gain insight into the structure of complexes **7** and **8**. The ^{1}H NMR spectrum of Re(I) complex **7** in CD_3OD shows two doublets at 8.29 and 7.11 ppm, each integrating for two protons, with a coupling constant of 6.4 Hz, consistent with the 2- and 3-

DOI: 10.1021/acs.inorgchem.8b00978
Inorg. Chem. XXXX, XXX, XXX−XXX

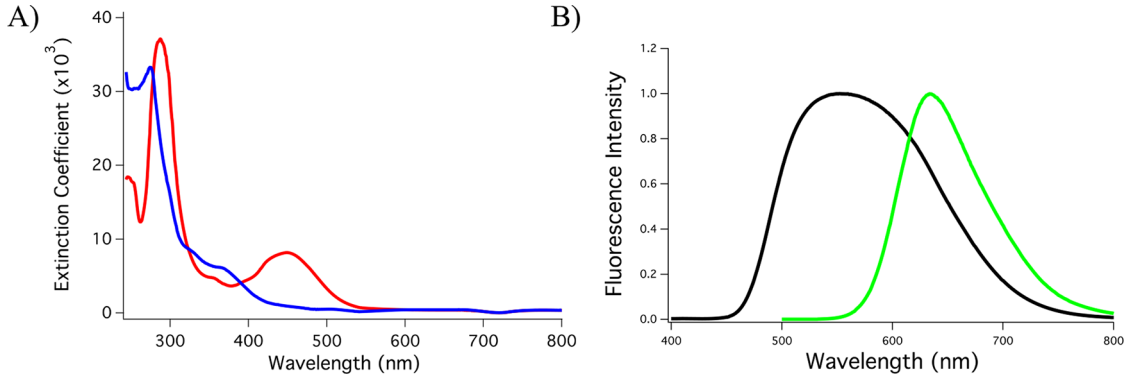

Figure 2. Electronic absorption spectra (A) and emission spectra (B) for **7** and **8**. Absorption spectra of **7** (blue) and **8** (red). Emission spectra of **7** (black) and **8** (green) were normalized and uncorrected.

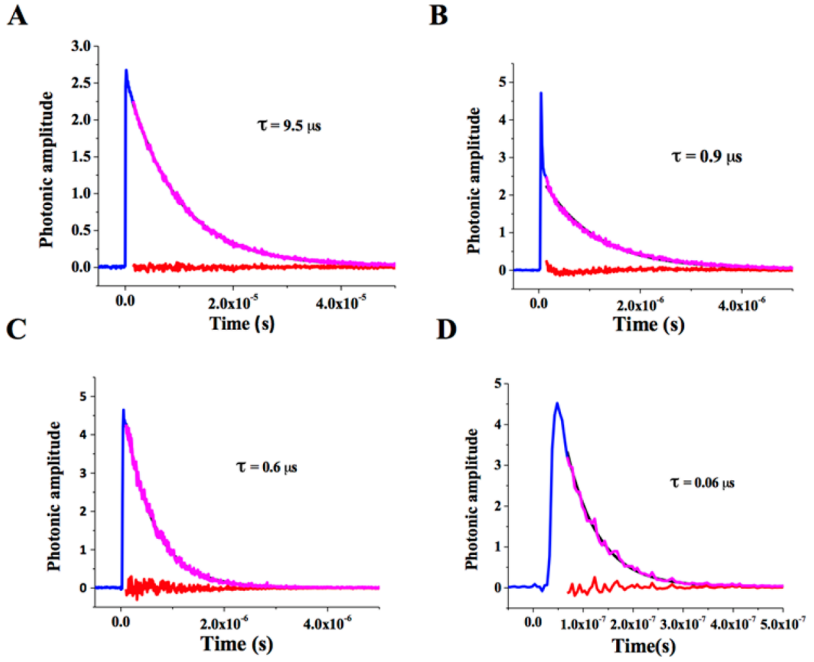

Figure 3. Emission decay of **7** and **8** at concentrations of 47.5 and 4.09 μM, respectively, at ambient temperature and 77 K (frozen solution) in potassium phosphate buffer 50 mM, pH 7.4, and 10% DMSO solvent using 337 nm pulsed excitation monitored at 543 and 631 nm: (A) **7** at 77 K; (B) **8** at 77 K; (C) **7** at ambient temperature; (D) **8** at ambient temperature. The monoexponential fit (black) and the extracted data (pink) are indistinguishable; residuals are shown in red. The samples were probably microcrystalline at 77 K. A fast decay component with about 10% of the substrate amplitude was probably mostly due to the instrument response to scattered excitation light, but it could also contain contribution from heterogeneities or impurities. Exponential decay fittings were performed in Origin; IRF = 12 ns.

Table 1. Kinetic and Thermodynamic Parameters for Inhibition of Cathepsins L, S, and B by 1, 2, 7, and 8[a]

	CTSL			CTSS			CTSB		
compd	K_i (μM)	k_{inact} (10^{-3} s^{-1})	k_{inact}/K_i (10^3 M^{-1} s^{-1})	K_i (μM)	k_{inact} (10^{-3} s^{-1})	k_{inact}/K_i (10^3 M^{-1} s^{-1})	K_i (μM)	k_{inact} (10^{-3} s^{-1})	k_{inact}/K_i (10^3 M^{-1} s^{-1})
1	0.77 ± 0.27[b]	11 ± 5[b]	13 ± 2.8[b]	105 ± 1	31 ± 8	0.29 ± 0.08	1933 ± 1573	2.1 ± 0.2	0.001
2	0.74 ± 0.05	31 ± 2	42.3 ± 4.1	3.0 ± 0.8	16 ± 1.3	5.3 ± 0.2	296 ± 8	2.7 ± 0.4	0.009
7	0.21 ± 0.04	43 ± 5	211 ± 42	9.4 ± 4.9	8.9 ± 4.6	0.95 ± 0.01	194 ± 23	0.2 ± 0.2	0.001
8	1.7 ± 0.4	14 ± 1	8.5 ± 2.5	3.3 ± 0.9	18 ± 3	5.5 ± 0.23	ND	ND	ND

[a]CSTL inhibition data were collected using CSTL (4 nM), *Z*-Phe-Arg-AMC (10 μM), **1**, **2**, **7**, and **8** (0.05−2.5 μM) in 0.4 M acetate buffer, pH 5.5, <1% DMSO, 4 mM EDTA, 0.01% Triton X-100, DTT 8 mM at 25 °C. CSTS inhibition data were collected using CSTS (4 nM), *Z*-Val-Val-Arg-AMC (10 μM), **1**, **2**, **7**, and **8** (1−20 μM) in 50 mM phosphate buffer, pH 6.5, <1% DMSO, 2.5 mM EDTA, DTT 8 mM at 25 °C. CSTB inhibition data were collected using CSTB (4 nM), *Z*-Arg-Arg-AMC (10 μM), **1**, **2**, **7**, and **8** (1 nM to 100 μM) in 0.4 M acetate buffer, pH 5.5, <1% DMSO, 5 mM EDTA, 0.01% Triton X-100, DTT 10 mM at 25 °C. CA-074 was used as a positive control for cathepsin B inhibition. Data are averages of three independent experiments with errors equal to standard deviations. [b]Data are from ref 34.

DOI: 10.1021/acs.inorgchem.8b00978
Inorg. Chem. XXXX, XXX, XXX−XXX

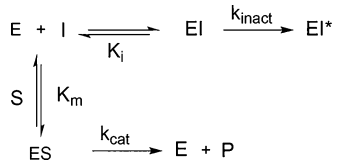

Figure 4. Model for competitive, irreversible inactivation of cathepsin L by epoxysuccinyl inhibitors with reversible formation of the enzyme inhibitor complex (EI) and irreversible formation of the covalent complex (EI*).

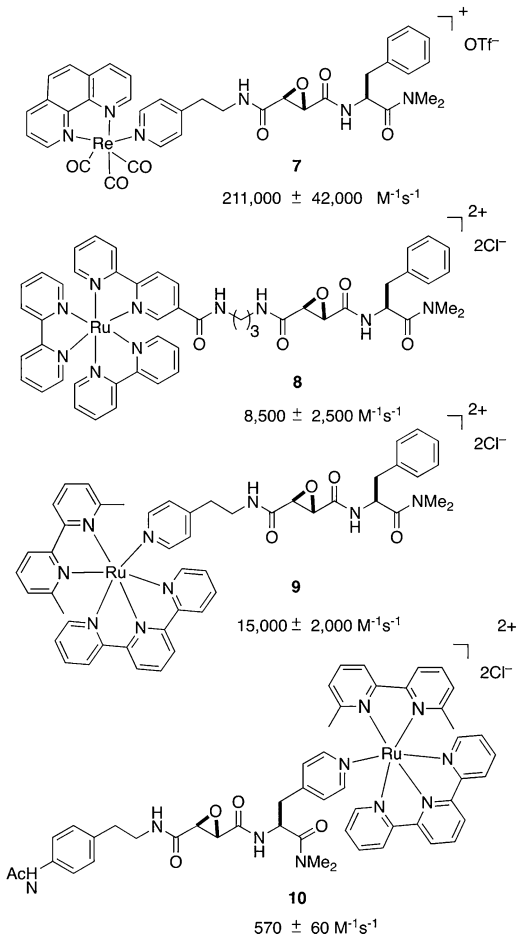

Figure 5. Re(I)- and Ru(II)-based inhibitors of CTSL **7**−**10** with second-order rate constants (k_{inact}/K_i) for irreversible enzyme inactivation. Data reveal that the nature of the metal complex and position of attachment strongly influence enzyme inhibition. Data for **9** and **10** are from ref 34.

pyridyl C−H groups of the pyridine ring. A triplet is observed at 5.06 ppm integrating for one proton consistent with the α-proton of the phenylalanine residue. In addition, two doublets with coupling constants of 1.5 Hz were observed at 3.25 and 3.14 ppm, each integrating for one proton, and are consistent with methine protons of the epoxide. Finally, doublets of doublets at 3.04 and 2.94 ppm, integrating for one proton each, were assigned as diastereotopic β-protons of the phenylalanine residue in **7**. Similar resonances were observed in the ^{1}H NMR spectrum of Ru(II) conjugate **8**, including a triplet of doublets at 5.08 ppm for the α-proton of the phenylalanine residue and one triplet and one doublet at 3.51 and 3.38 ppm, respectively, corresponding to the methine protons of the epoxide. The triplet at 3.51 ppm has a coupling constant of 2 Hz and is likely

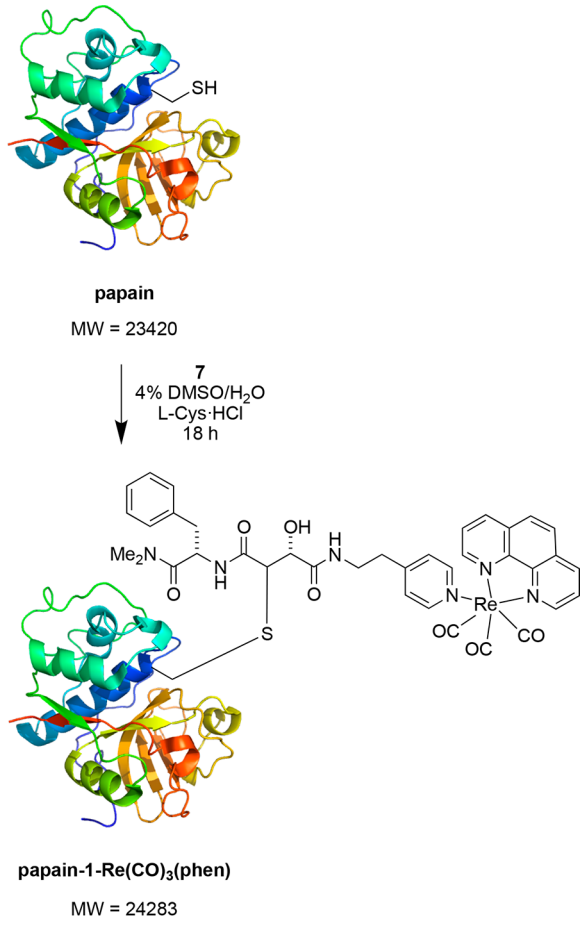

Figure 6. Preparation of a papain-**7** conjugate and characterization by ESMS revealing that the Re(I)(phen)$(CO)_3$ metal fragment remains intact upon covalent modification of papain by **7**.

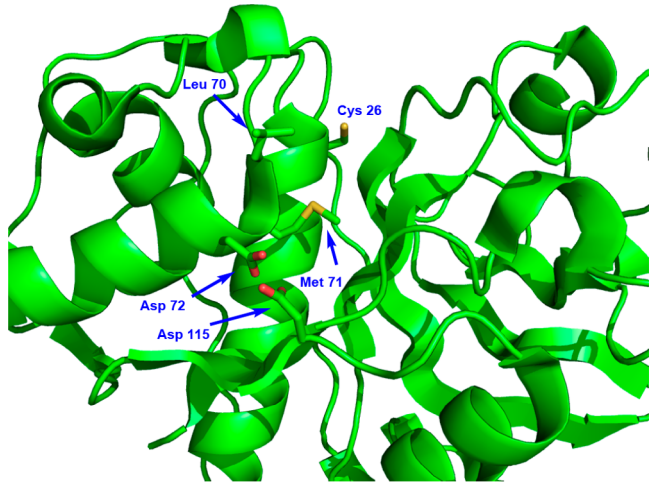

Figure 7. Model of CSTL adapted from PDB 3OF8 showing location of key residues in the S3 subsite.[51]

the result of merging of two doublets with coupling constants of ∼2 Hz; one coupling constant is attributed to an adjacent methine proton and the other 2 Hz coupling constant is presumably ^5J coupling with a disatereotopic CH proton adjacent to NH. The IR spectrum of **7** demonstrates ν_{CO} stretches at 2029 and 1906 cm^{-1}, indicating the presence of the *fac*-[Re$(CO)_3$] core.[44]

DOI: 10.1021/acs.inorgchem.8b00978
Inorg. Chem. XXXX, XXX, XXX−XXX

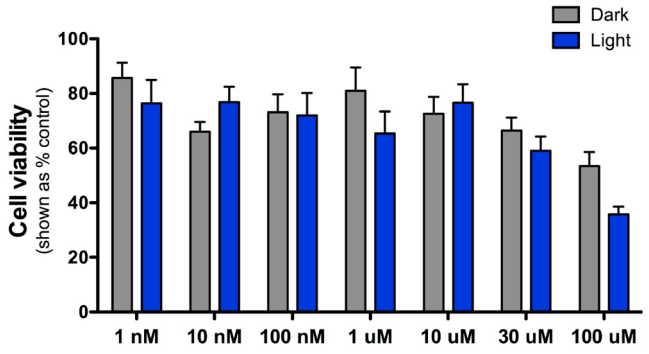

Figure 8. Viability of DU145 cells in response to compound **7**. The cell viability was determined by MTT assay after 48 h and is reported relative to control with only the vehicle (0.5% DMSO) added. Cells were incubated in the presence of **7** (1 nM to 100 μM) at 37 °C for 2 h, followed by 40 min incubation in the dark at room temperature or irradiated with a 4 W long-wave UV (365 nm) light, powered at 115 V. Error bars represent the standard error of the mean of eight replicate wells, and data are representative of three independent experiments.

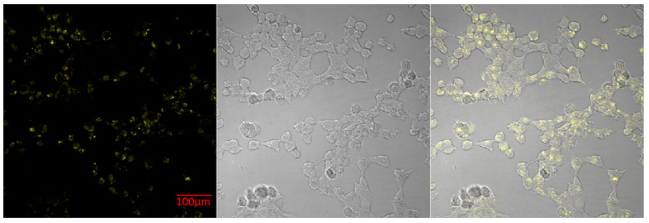

Figure 9. Confocal images of live DU-145 cells treated with **7** (30 μM): fluorescence (left), bright field microscopy (middle), and overlay (right).

Lifetime Measurements. Emission lifetimes for **7** and **8** at concentrations of 47.5 and 4.09 μM, respectively, were determined in PBS buffer (pH 7.4, 10% DMSO) at 77 K (frozen solution) and under ambient conditions (Figure 3). Complexes **7** and **8** were monitored for emission at 543 and 631 nm, respectively, following irradiation at 337 nm (pulse width 5 ns). The monoexponential fits (black) and original signal (blue) are indistinguishable; residuals are shown in red. Lifetimes determined for **7** were 9.50 $\pm$ 0.2 μs at 77 K and 0.60 $\pm$ 0.02 μs at 293 $\pm$ 2 K. Shorter lifetimes were observed for Ru(II)-based **8**: 0.90 $\pm$ 0.05 μs at 77 K and 0.06 $\pm$ 0.02 μs at 293 $\pm$ 2 K. The monoexponential fits (black) and original signal (blue) are indistinguishable; residuals are shown in red (Figure 3). These data confirm that **7** and **8** have excited state lifetimes significantly longer than those of endogenous fluorophores that contribute to autofluorescence (<10 ns), giving the Re and Ru conjugates potential for use in time-gated imaging experiments.[30]

Enzyme Inhibition. Compounds **1**, **2**, **7**, and **8** were evaluated for inhibition of cysteine cathepsins B (CTSB), L (CTSL), and S (CTSS) to determine how attachment of the metal complexes influenced enzyme inhibition. All three enzymes are endopeptidases that are abundantly expressed in a variety of human tissues.[45] In addition, CTSB also shows dicarboxypeptidase activity.[3,46] Cathepsin inhibition was measured using progress curve assays with continuous monitoring of fluorogenic substrate hydrolysis. Solutions of aminomethylcoumarin (AMC)-based fluorogenic substrates (10 μM) and inhibitor (0.05–20 μM) in 50 mM phosphate or 0.4 M acetate buffer (see Table 1 for exact conditions) were treated with the enzyme CTSL, CTSS, or CTSB (4 nM) activated with DTT (8 mM) and were immediately analyzed for formation of free AMC over the course of 15 min. Data

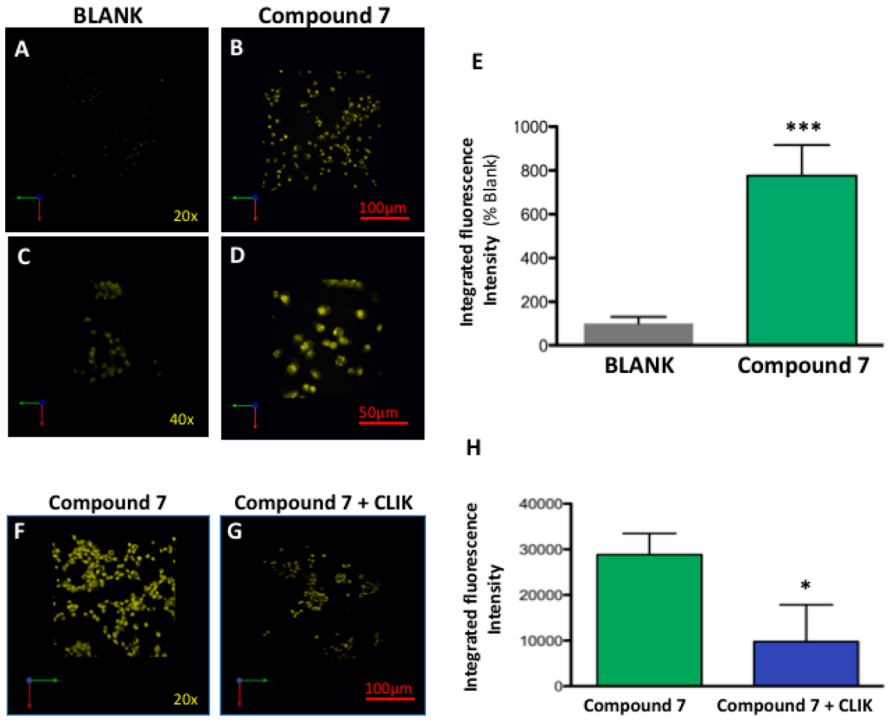

Figure 10. Uptake of **7** by living prostate cancer cells: (A–D) Volocity export images of untreated (blank; A, C) and **7**-treated (30 μM, B, D) DU-145 cells; (E) Quantification of intracellular fluorescence intensity upon compound **7** treatment; (F–H) reduction of intracellular fluorescence with cathepsin L inhibition by pretreatment with CLIK-148 (50 μM) for 24 h before **7** (30 μM).

DOI: 10.1021/acs.inorgchem.8b00978
Inorg. Chem. XXXX, XXX, XXX–XXX

were fit to a standard two-step model for irreversible enzyme inhibition, where noncovalent binding of the inhibitor and irreversible covalent bond formation to form the inactivated enzyme EI* compete with hydrolysis of substrate S to form product P (Figure 4). By following substrate hydrolysis over time in the presence of variable amounts of inhibitor, the thermodynamics of reversible inhibitor binding (K_i) and the rate constant for irreversible covalent bond formation with the inhibitor (k_{inact}) can be obtained. The quotient k_{inact}/K_i is an important parameter that is often used as a measure of potency and represents the second-order rate constant for enzyme inactivation by the irreversible inhibitor.

Inhibition data for compounds **1**, **2**, **7**, and **8** of CTSL, CTSS, and CTSB are presented in Table 1. Inhibitor **1** gave k_{inact}/K_i = 13000 ± 2800 M^{-1} s^{-1}, which is within experimental error of the value for the potent CTSL inhibitor CLIK-148 (11000 ± 3000 M^{-1} s^{-1}).[47] The bipyidine derivative **2** showed K_i = 0.74 ± 0.05 μM, similar to that of **1**, but demonstrated a significantly higher rate of irreversible inactivation (k_{inact} = 0.031 ± 0.002 s^{-1}) in comparison to **1**, which gave a k_{inact}/K_i value for **2** for CTSL inactivation roughly 3 times that of **1**. Both compounds **1** and **2** were selective for CTSL over the related cysteine protease CTSS, with k_{inact}/K_i ratios for CTSL/CTSS of 45 and 8, respectively. Neither **1** nor **2** inhibited CTSB potently, with k_{inact}/K_i values of around 1.00 M^{-1} s^{-1}. Interestingly, compound **7**, the Re(phen)$(CO)_3$ conjugate of **1**, was much more potent than **1** and **2**, with a second-order rate constant of 211000 ± 42000 M^{-1} s^{-1}, greater than 16 times that for **1**. This makes **7** among the most potent irreversible CTSL inhibitors known to date.[18,48] Data revealed that the higher potency for **7** vs **1** was due to tighter reversible binding (~4-fold) and faster inactivation (~4-fold). In addition, **7** showed an enhanced selectivity over **1** for CTSL vs CTSS inhibition, increasing the CTSL/CTSS k_{inact}/K_i ratio from 45 with **1** to 222 for **7**. In other words, attaching the Re(phen)$(CO)_3$ unit to **1** improved both potency and selectivity for inhibition of CTSL over CTSS. Like **1** and **2**, Re(I) compound **7** was not a potent inhibitor of CTSB. Ru(II)-based compound **8** showed behavior very different from **7**. First, **8** was roughly 25 times less potent against CTSL than **7**, with a k_{inact}/K_i value of only 8500 ± 2500 M^{-1} s^{-1}. Second, attaching the Ru$(bpy)_2$ fragment to **2** to give **8** actually decreased rather than increased the k_{inact}/K_i value for **8** relative to **2** by a factor of almost 5. Third, the selectivity for CTSL over CTSS was eroded for **8**, with a ratio of only 1.5, in comparison to 222 for **7**.

Taken together with data from previously synthesized metal−inhibitor conjugates (Figure 5),[34] our results collectively confirm that the position and nature of the metal center strongly influence potency and selectivity of CTSL inhibition. A comparison of conjugates **7** and **9**, which contain the same parent inhibitor structure but different metal fragments, Re(phen)$(CO)_3$ and Ru(tpy)(Me_2bpy), respectively, indicates that the Re(I) group is much better tolerated than the more bulky Ru(II) fragment in the CTSL active site. Compounds **8** and **9** have Ru(II) fragments with similar size but different linker lengths between the epoxysuccinyl group and the metal center and differ by a factor of less than 2 for k_{inact}/K_i values, suggesting that hydrophobic cationic groups are tolerated reasonably well by CTSL. In contrast, placing Ru(tpy)-(Me_2bpy) on the pyridylalanine side chain of **10** strongly decreases the rate of inhibitor inactivation, with a k_{inact}/K_i value of only 570 ± 60 M^{-1} s^{-1}.

Mechanism of Enzyme Inhibition. Literature data reveal that rhenium compounds, specifically Re(V)−oxo complexes, are potent inhibitors of cysteine proteases.[27] In these cases, the rhenium metal center undergoes direct ligation to the nucleophilic thiolate in the cysteine protease active site. To gain further insight into the mode of inhibition of CTSL by **7**, several more experiments were carried out. The complex [Re(phen)$(CO)_3$(pyridine)](OTf)[49] was used as a control to probe for potential rhenium binding but showed no inhibition of CTSL at concentrations up to 100 μM, in stark contrast with **7**, which inhibits CTSL in the low-nanomolar range. Binding of **7** to the cysteine protease papain, a close model of CTSL,[50] was probed by MS analysis. Treatment of papain with excess **7**, followed by isolation through a size exclusion filter and ESMS analysis, revealed a major product with MW = 24283 (Figures S24 and S25), consistent with the calculated mass for the papain-**1**-[Re(phen)$(CO)_3$] adduct (Figure 6). These data are consistent with the epoxysuccinyl group, rather than the Re(I) metal center, forming a covalent bond with inhibitor **7** through attack of the active site thiolate on the epoxide, resulting in ring opening. Taken together, these data indicate that the Re complex of **7** remains intact and does not undergo ligand substitution due to direct binding to the thiolate. Instead, the enhancement of inhibition observed between **1** and **7** is likely due to favorable noncovalent interactions between the cationic Re(I) metal complex and CTSL, likely a carboxylate-rich area near the S3 subsite (Figure 7).

Cellular Studies. Rhenium conjugates of biologically active molecules have shown great success in cell imaging experiments.[29,30,33,52−61] To probe whether compound **7** would be appropriate for cell imaging experiments, we used DU-145 cancer cells, an aggressive form of prostate cancer cells that are known to express high levels of CTSL in culture.[62] First, we assessed the effects of **7** on cell viability. Re(I) complex **7** was well tolerated by the DU-145 cells, with only minor toxicity observed, except at the highest concentration surveyed (100 μM) under light (365 nm irradiation) or dark conditions (Figure 8), as judged by the MTT assay after 48 h.

Next, DU-145 cells were treated with **7** (30 μM) for 2 h under regular growth conditions and then washed with PBS buffer and imaged by confocal microscopy, using 405 nm excitation. Compound **7** clearly caused a significant increase in intracellular fluorescence intensity (Figure 9). To probe for CTSL binding, DU-145 cells were treated with the CTSL-selective inhibitor CLIK-148 (50 μM) for 24 h prior to treating with **7** (30 μM). Intracellular fluorescence intensity decreased significantly by over 50%, consistent with CLIK-148 and **7** competing for the same binding sites (Figure 10). These data are consistent with **7** being nontoxic, cell-permeable, and able to label active CTSL in living prostate cancer cells.

In order to further probe for the selectivity of CTSL binding, Re(I) compound **7** was evaluated by SDS-PAGE analysis of cell lysates from DU-145 and ARCaP(M) prostate cancer cells, which both express high levels of CTSL. First, the lysates were prepared and assayed for activity of CTSL using progressive curves for hydrolysis of *Z*-Phe-Arg-AMC. Fluorescence readings increased linearly 2.6-fold in PC3 and 3-fold in ARCaP(M) over the course of 15 min, demonstrating that CTSL is active in both cell lysates. With lysates containing catalytically active CTSL in hand, samples were incubated with 5 μM [Re(phen)-$(CO)_3$(**1**)](OTf) (**7**) for 15 min and then heated for 5 min at 100 °C and analyzed by SDS PAGE gel analysis. Unfortunately, we unable to detect a fluorescent band corresponding to the

DOI: 10.1021/acs.inorgchem.8b00978
Inorg. Chem. XXXX, XXX, XXX−XXX

labeled CTSL (37 kDa) or any other larger proteins by gel analysis. Instead, we detected a fluorescent band moving at the dye front (<8 kDa). Similar experiments at higher concentrations of **7** (30 μM) with and without boiling the sample before analysis were conducted but gave the same results. We considered that the covalent cathepsin L-**7** adduct might not be stable to gel analysis, presumably because it is electrochemically active, and labile and is released from the monopyridine donor upon subjection to SDS-PAGE analysis. Even though our data confirmed that **7** is a highly potent, selective, and irreversible inhibitor of CTSL that is cell permeable, further experiments will be needed to confirm the selectivity of **7** for labeling CTSL in the presence of other proteins, as present in the complex milieu of lysates and whole cells.

CONCLUSION

In conclusion, we report a Re(I)-based inhibitor of CTSL that is highly potent, selective, and cell permeable. Our data are consistent with the Re(I) complex enhancing binding to CTSL and increasing the rate of irreversible alkylation, making **7** among the most potent inhibitors of CTSL recorded to date. Importantly, this study reveals a new strategy for using coordinatively saturated metal complexes to enhance potency and selectivity of inhibitors through favorable noncovalent interactions using metal centers. This strategy is novel and distinct from using complexes with vacant coordination sites as enzyme inhibitors to ligate nucleophilic enzyme side chains or complexes that bind directly inside active sites.[63,64] Given that transition metals such as Re are not native in biology and are subject to nontraditional methods for quantification and imaging, such as ICP-MS and IR-based spectromicroscopy, **7** and derivatives thereof may hold promise as reagents for enzyme inhibition, detection, and quantification.

ASSOCIATED CONTENT

Supporting Information

The Supporting Information is available free of charge on the ACS Publications website at DOI: 10.1021/acs.inorgchem.8b00978.

^{1}H and ^{13}C NMR and HRMS spectra for new compounds, enzyme inhibition studies, papain rhenium conjugate and MS analysis, and lifetime measurements (PDF)

AUTHOR INFORMATION

Corresponding Author

*E-mail for J.J.K.: jkodanko@chem.wayne.edu.

ORCID

John Endicott: 0000-0002-8998-1030

Jeremy J. Kodanko: 0000-0001-5196-7463

Notes

The authors declare no competing financial interest.

ACKNOWLEDGMENTS

We gratefully acknowledge the National Institutes of Health (Grant EB 016062) and Wayne State University for their generous support of this research.

REFERENCES

(1) Turk, V.; Stoka, V.; Vasiljeva, O.; Renko, M.; Sun, T.; Turk, B.; Turk, D. Cysteine cathepsins: From structure, function and regulation to new frontiers. *Biochim. Biophys. Acta, Proteins Proteomics* **2012**, *1824* (1), 68−88.

(2) Joyce, J. A.; Hanahan, D. Multiple roles for cysteine cathepsins in cancer. *Cell Cycle* **2004**, *3* (12), 1516−1519.

(3) Mohamed, M. M.; Sloane, B. F. Cysteine cathepsins: multifunctional enzymes in cancer. *Nat. Rev. Cancer* **2006**, *6* (10), 764−775.

(4) Katunuma, N. Structure-based development of specific inhibitors for individual cathepsins and their medical applications. *Proc. Jpn. Acad., Ser. B* **2011**, *87* (2), 29−39.

(5) Turk, B. Targeting proteases: successes, failures and future prospects. *Nat. Rev. Drug Discovery* **2006**, *5* (9), 785−799.

(6) Otto, H.-H.; Schirmeister, T. Cysteine Proteases and Their Inhibitors. *Chem. Rev.* **1997**, *97* (1), 133−171.

(7) Sudhan, D. R.; Siemann, D. W. Cathepsin L targeting in cancer treatment. *Pharmacol. Ther.* **2015**, *155*, 105−116.

(8) Li, W.; Kornmark, L.; Jonasson, L.; Forssell, C.; Yuan, X.-M. Cathepsin L is significantly associated with apoptosis and plaque destabilization in human atherosclerosis. *Atherosclerosis* **2009**, *202* (1), 92−102.

(9) Mattock, K. L.; Gough, P. J.; Humphries, J.; Burnand, K.; Patel, L.; Suckling, K. E.; Cuello, F.; Watts, C.; Gautel, M.; Avkiran, M.; Smith, A. Legumain and cathepsin-L expression in human unstable carotid plaque. *Atherosclerosis* **2010**, *208* (1), 83−89.

(10) Conus, S.; Simon, H.-U. Cathepsins and their involvement in immune responses. *Swiss Med. Wkly.* **2010**, *140* (July), 4−11.

(11) Wartmann, T.; Mayerle, J.; Kaehne, T.; Sahin-Toth, M.; Ruthenbuerger, M.; Matthias, R.; Kruse, A.; Reinheckel, T.; Peters, C.; Weiss, F. U.; Sendler, M.; Lippert, H.; Schulz, H.-U.; Aghdassi, A.; Dummer, A.; Teller, S.; Halangk, W.; Lerch, M. M. Cathepsin L inactivates human trypsinogen, whereas cathepsin L-deletion reduces the severity of pancreatitis in mice. *Gastroenterology* **2010**, *138* (2), 726−737.

(12) Strojnik, T.; Kavalar, R.; Trinkaus, M.; Lah, T. T. Cathepsin L in glioma progression: Comparison with cathepsin B. *Cancer Detect. Prev.* **2005**, *29* (5), 448−455.

(13) Lankelma, J. M.; Voorend, D. M.; Barwari, T.; Koetsveld, J.; Van der Spek, A. H.; De Porto, A. P. N. A.; Van Rooijen, G.; Van Noorden, C. J. F. Cathepsin L, target in cancer treatment? *Life Sci.* **2010**, *86* (7−8), 225−233.

(14) Palermo, C.; Joyce, J. A. Cysteine cathepsin proteases as pharmacological targets in cancer. *Trends Pharmacol. Sci.* **2008**, *29* (1), 22−28.

(15) Blum, G.; von Degenfeld, G.; Merchant, M. J.; Blau, H. M.; Bogyo, M. Noninvasive optical imaging of cysteine protease activity using fluorescently quenched activity-based probes. *Nat. Chem. Biol.* **2007**, *3* (10), 668−677.

(16) Verdoes, M.; Oresic Bender, K.; Segal, E.; van der Linden, W. A.; Syed, S.; Withana, N. P.; Sanman, L. E.; Bogyo, M. Improved Quenched Fluorescent Probe for Imaging of Cysteine Cathepsin Activity. *J. Am. Chem. Soc.* **2013**, *135* (39), 14726−14730.

(17) Ben-Nun, Y.; Merquiol, E.; Brandis, A.; Turk, B.; Scherz, A.; Blum, G. Photodynamic quenched cathepsin activity based probes for cancer detection and macrophage targeted therapy. *Theranostics* **2015**, *5* (8), 847−862.

(18) Powers, J. C.; Asgian, J. L.; Ekici, O. D.; James, K. E. Irreversible inhibitors of serine, cysteine, and threonine proteases. *Chem. Rev.* **2002**, *102* (12), 4639−4750.

(19) Frizler, M.; Stirnberg, M.; Sisay, M. T.; Guetschow, M. Development of nitrile-based peptidic inhibitors of cysteine cathepsins. *Curr. Top. Med. Chem.* **2010**, *10* (3), 294−322.

(20) Katunuma, N.; Murata, E.; Kakegawa, H.; Matsui, A.; Tsuzuki, H.; Tsuge, H.; Turk, D.; Turk, V.; Fukushima, M.; Tada, Y.; Asao, T. Structure based development of novel specific inhibitors for cathepsin L and cathepsin S in vitro and in vivo. *FEBS Lett.* **1999**, *458* (1), 6−10.

(21) Kellett, A.; Prisecaru, A.; Slator, C.; Molphy, Z.; McCann, M. Metal-Based Antimicrobial Protease Inhibitors. *Curr. Med. Chem.* **2013**, *20* (25), 3134−3151.

(22) Fricker, S. P.; Mosi, R. M.; Cameron, B. R.; Baird, I.; Zhu, Y.; Anastassov, V.; Cox, J.; Doyle, P. S.; Hansell, E.; Lau, G.; Langille, J.;

DOI: 10.1021/acs.inorgchem.8b00978
Inorg. Chem. XXXX, XXX, XXX−XXX

Olsen, M.; Qin, L.; Skerlj, R.; Wong, R. S. Y.; Santucci, Z.; McKerrow, J. H. Metal compounds for the treatment of parasitic diseases. *J. Inorg. Biochem.* **2008**, *102* (10), 1839−1845.
(23) Bincoletto, C.; Tersariol, I. L. S.; Oliveira, C. R.; Dreher, S.; Fausto, D. M.; Soufen, M. A.; Nascimento, F. D.; Caires, A. C. F. Chiral cyclopalladated complexes derived from N,N-dimethyl-1-phenethylamine with bridging bis(diphenylphosphine)ferrocene ligand as inhibitors of the cathepsin B activity and as antitumoral agents. *Bioorg. Med. Chem.* **2005**, *13* (8), 3047−3055.
(24) Zhu, Y.; Cameron, B. R.; Skerlj, R. T. Cycloauration of substituted 2-phenoxypyridine derivatives and X-ray crystal structure of gold, dichloro[2-[[5-[(cyclopentylamino)carbonyl]-2-pyridinyl-κN]oxy]phenyl-κC]-, (SP-4−3). *J. Organomet. Chem.* **2003**, *677* (1−2), 57−72.
(25) Baird, I. R.; Mosi, R.; Olsen, M.; Cameron, B. R.; Fricker, S. P.; Skerlj, R. T. '3 + 1' Mixed-ligand oxorhenium(V) complexes and their inhibition of the cysteine proteases cathepsin B and cathepsin K. *Inorg. Chim. Acta* **2006**, *359* (9), 2736−2750.
(26) Mosi, R.; Baird, I. R.; Cox, J.; Anastassov, V.; Cameron, B.; Skerlj, R. T.; Fricker, S. P. Rhenium Inhibitors of Cathepsin B (ReO(SYS)X (Where Y = S, py; X = Cl, Br, SPhOMe-p)): Synthesis and Mechanism of Inhibition. *J. Med. Chem.* **2006**, *49* (17), 5262−5272.
(27) Fricker, S. P. Cysteine proteases as targets for metal-based drugs. *Metallomics* **2010**, *2* (6), 366−377.
(28) Zhu, Y.; Cameron, B. R.; Mosi, R.; Anastassov, V.; Cox, J.; Qin, L.; Santucci, Z.; Metz, M.; Skerlj, R. T.; Fricker, S. P. Inhibition of the cathepsin cysteine proteases B and K by square-planar cycloaurated gold(III) compounds and investigation of their anti-cancer activity. *J. Inorg. Biochem.* **2011**, *105* (5), 754−762.
(29) Lo, K. K.-W. Luminescent Rhenium(I) and Iridium(III) Polypyridine Complexes as Biological Probes, Imaging Reagents, and Photocytotoxic Agents. *Acc. Chem. Res.* **2015**, *48* (12), 2985−2995.
(30) Marti, A. A. Metal complexes and time-resolved photoluminescence spectroscopy for sensing applications. *J. Photochem. Photobiol., A* **2015**, *307*−*308*, 35−47.
(31) Baggaley, E.; Weinstein, J. A.; Williams, J. A. G. Lighting the way to see inside the live cell with luminescent transition metal complexes. *Coord. Chem. Rev.* **2012**, *256* (15−16), 1762−1785.
(32) Haas, K. L.; Franz, K. J. Application of Metal Coordination Chemistry To Explore and Manipulate Cell Biology. *Chem. Rev.* **2009**, *109* (10), 4921−4960.
(33) Hostachy, S.; Policar, C.; Delsuc, N. Re(I) carbonyl complexes: Multimodal platforms for inorganic chemical biology. *Coord. Chem. Rev.* **2017**, *351*, 172−188.
(34) Huisman, M.; Lewalski, V. G.; Kodanko, J. J.; White, J. K.; Turro, C.; Podgorski, I. Caging the uncageable: using metal complex release for photochemical control over irreversible inhibition. *Chem. Commun.* **2016**, *52* (85), 12590−12593.
(35) Kiehne, U.; Bunzen, J.; Staats, H.; Luetzen, A. Synthesis of substituted 2,2'-bipyridines from 2-bromo- or 2-chloropyridines using tetrakis(triphenylphosphine)palladium(0) as a catalyst in a modified Negishi cross-coupling reaction. *Synthesis* **2007**, *2007* (7), 1061−1069.
(36) Kuss-Petermann, M.; Wolf, H.; Stalke, D.; Wenger, O. S. Influence of Donor−Acceptor Distance Variation on Photoinduced Electron and Proton Transfer in Rhenium(I)−Phenol Dyads. *J. Am. Chem. Soc.* **2012**, *134* (30), 12844−12854.
(37) Al-Rawashdeh, N. A. F.; Chatterjee, S.; Krause, J. A.; Connick, W. B. Ruthenium Bis-diimine Complexes with a Chelating Thioether Ligand: Delineating 1,10-Phenanthrolinyl and 2,2′-Bipyridyl Ligand Substituent Effects. *Inorg. Chem.* **2014**, *53* (1), 294−307.
(38) Mazumder, S.; Thomas, R. A.; Lord, R. L.; Schlegel, H. B.; Endicott, J. F. A density functional theory and spectroscopic study of intramolecular quenching of metal-to-ligand charge-transfer excited states in some mono-bipyridine ruthenium(II) complexes. *Can. J. Chem.* **2014**, *92* (10), 996−1009.
(39) Kuzmic, P. Program DYNAFIT for the analysis of enzyme kinetic data: application to HIV proteinase. *Anal. Biochem.* **1996**, *237* (2), 260−273.
(40) Zhou, X.; Liu, W.-J.; Ye, J.-L.; Huang, P.-Q. A versatile approach to pyrrolidine azasugars and homoazasugars based on a highly diastereoselective reductive benzyloxymethylation of protected tartarimide. *Tetrahedron* **2007**, *63* (27), 6346−6357.
(41) Chehade, K. A. H.; Baruch, A.; Verhelst, S. H. L.; Bogyo, M. An improved preparation of the activity-based probe JPM-OEt and in situ applications. *Synthesis* **2005**, *2005*, 240−244.
(42) Sacksteder, L.; Zipp, A. P.; Brown, E. A.; Streich, J.; Demas, J. N.; DeGraff, B. A. Luminescence studies of pyridine.alpha.-diimine rhenium(I) tricarbonyl complexes. *Inorg. Chem.* **1990**, *29* (21), 4335−4340.
(43) Cook, M. J.; Lewis, A. P.; McAuliffe, G. S. G.; Skarda, V.; Thomson, A. J.; Glasper, J. L.; Robbins, D. J. Luminescent metal complexes. Part 1. Tris-chelates of substituted 2,2'-bipyridyls with ruthenium(II) as dyes for luminescent solar collectors. *J. Chem. Soc., Perkin Trans. 2* **1984**, No. 8, 1293−1301.
(44) Kam-Wing Lo, K.; Chun-Ming Ng, D.; Hui, W.-K.; Cheung, K.-K. Luminescent rhenium(I) polypyridine complexes with an isothiocyanate moiety-versatile labeling reagents for biomolecules. *J. Chem. Soc., Dalton Trans.* **2001**, *18*, 2634−2640.
(45) Brix, K.; Dunkhorst, A.; Mayer, K.; Jordans, S. Cysteine cathepsins: Cellular roadmap to different functions. *Biochimie* **2008**, *90* (2), 194−207.
(46) Olson, O. C.; Joyce, J. A. Cysteine cathepsin proteases: regulators of cancer progression and therapeutic response. *Nat. Rev. Cancer* **2015**, *15* (12), 712−729.
(47) Katunuma, N.; Tsuge, H.; Nukatsuka, M.; Fukushima, M. Structure-based development of cathepsin L inhibitors and therapeutic applications for prevention of cancer metastasis and cancer-induced osteoporosis. *Adv. Enzyme Regul.* **2002**, *42*, 159−172.
(48) Schaschke, N.; Assfalg-Machleidt, I.; Machleidt, W. Inhibition of cathepsin L by epoxysuccinyl peptides simultaneously addressing active-site and remote-site regions. *ChemBioChem* **2008**, *9* (11), 1721−1724.
(49) Hanss, D.; Walther, M. E.; Wenger, O. S. Accelerated hole transfer across a molecular double barrier. *Chem. Commun.* **2010**, *46* (37), 7034−7036.
(50) Tsuge, H.; Nishimura, T.; Tada, Y.; Asao, T.; Turk, D.; Turk, V.; Katunuma, N. Inhibition Mechanism of Cathepsin L-Specific Inhibitors Based on the Crystal Structure of Papain-CLIK148 Complex. *Biochem. Biophys. Res. Commun.* **1999**, *266* (2), 411−416.
(51) Fujishima, A.; Imai, Y.; Nomura, T.; Fujisawa, Y.; Yamamoto, Y.; Sugawara, T. The crystal structure of human cathepsin L complexed with E-64. *FEBS Lett.* **1997**, *407* (1), 47−50.
(52) Carrington, S. J.; Chakraborty, I.; Mascharak, P. K.; Bernard, J. M. L. A Theranostic Two-Tone Luminescent PhotoCORM Derived from Re(I) and (2-Pyridyl)-benzothiazole: Trackable CO Delivery to Malignant Cells. *Inorg. Chem.* **2016**, *55* (16), 7852−7858.
(53) Choi, A. W.-T.; Louie, M.-W.; Li, S. P.-Y.; Liu, H.-W.; Chan, B. T.-N.; Lam, T. C.-Y.; Lin, A. C.-C.; Cheng, S.-H.; Lo, K. K.-W. Emissive Behavior, Cytotoxic Activity, Cellular Uptake, and PEGylation Properties of New Luminescent Rhenium(I) Polypyridine Poly(ethylene glycol) Complexes. *Inorg. Chem.* **2012**, *51* (24), 13289−13302.
(54) Lo, K. K.-W.; Zhang, K. Y.; Li, S. P.-Y. Recent Exploitation of Luminescent Rhenium(I) Tricarbonyl Polypyridine Complexes as Biomolecular and Cellular Probes. *Eur. J. Inorg. Chem.* **2011**, *2011* (24), 3551−3568.
(55) Pierri, A. E.; Pallaoro, A.; Wu, G.; Ford, P. C. A Luminescent and Biocompatible PhotoCORM. *J. Am. Chem. Soc.* **2012**, *134* (44), 18197−18200.
(56) Prieto, L.; Rossier, J.; Derszniak, K.; Dybas, J.; Oetterli, R. M.; Kottelat, E.; Chlopicki, S.; Zelder, F.; Zobi, F. Modified biovectors for the tuneable activation of anti-platelet carbon monoxide release. *Chem. Commun.* **2017**, *53* (51), 6840−6843.
(57) Yempally, V.; Kyran, S. J.; Raju, R. K.; Fan, W. Y.; Brothers, E. N.; Darensbourg, D. J.; Bengali, A. A. Thermal and Photochemical Reactivity of Manganese Tricarbonyl and Tetracarbonyl Complexes

DOI: 10.1021/acs.inorgchem.8b00978
Inorg. Chem. XXXX, XXX, XXX−XXX

with a Bulky Diazabutadiene Ligand. *Inorg. Chem.* **2014**, *53* (8), 4081−4088.
(58) Zhang, K. Y.; Tso, K. K.-S.; Louie, M.-W.; Liu, H.-W.; Lo, K. K.-W. A Phosphorescent Rhenium(I) Tricarbonyl Polypyridine Complex Appended with a Fructose Pendant That Exhibits Photocytotoxicity and Enhanced Uptake by Breast Cancer Cells. *Organometallics* **2013**, *32* (18), 5098−5102.
(59) Zobi, F.; Degonda, A.; Schaub, M. C.; Bogdanova, A. Y. CO Releasing Properties and Cytoprotective Effect of cis-trans-[ReII-(CO)2Br2L2]n Complexes. *Inorg. Chem.* **2010**, *49* (16), 7313−7322.
(60) Choi, A. W.-T.; Tso, K. K.-S.; Yim, V. M.-W.; Liu, H.-W.; Lo, K. K.-W. Modification of 1,2,4,5-tetrazine with cationic rhenium(I) polypyridine units to afford phosphorogenic bioorthogonal probes with enhanced reaction kinetics. *Chem. Commun.* **2015**, *51* (16), 3442−3445.
(61) Ye, R.-R.; Tan, C.-P.; Lin, Y.-N.; Ji, L.-N.; Mao, Z.-W. A phosphorescent rhenium(I) histone deacetylase inhibitor: mitochondrial targeting and paraptosis induction. *Chem. Commun.* **2015**, *51* (39), 8353−8356.
(62) Friedrich, B.; Jung, K.; Lein, M.; Turk, I.; Rudolph, B.; Hampel, G.; Schnorr, D.; Loening, S. A. Cathepsins B, H, L and cysteine protease inhibitors in malignant prostate cell lines, primary cultured prostatic cells and prostatic tissue. *Eur. J. Cancer* **1999**, *35* (1), 138−144.
(63) Louie, A. Y.; Meade, T. J. Metal Complexes as Enzyme Inhibitors. *Chem. Rev.* **1999**, *99* (9), 2711−2734.
(64) Meggers, E. Targeting proteins with metal complexes. *Chem. Commun.* **2009**, *9*, 1001−1010.

DOI: 10.1021/acs.inorgchem.8b00978
Inorg. Chem. XXXX, XXX, XXX−XXX